Development of an Improved Prediction Model for Indoor Rolling Noise

Matthew Edwards, Fabien Chevillotte, François-Xavier Bécot, Luc Jaouen, Nicolas Totaro

DEVELOPMENT OF AN IMPROVED PREDICTION MODEL FOR INDOOR ROLLING NOISE

M. Edwards[1] **F. Chevillotte**[1] **F.-X. Bécot**[1]
L. Jaouen[1] **N. Totaro**[2]
[1] Matelys Research Lab, 7 Rue des Maraîchers, Bât B, 69120 Vaulx-en-Velin , France
[2] INSA—Lyon 20 Avenue Albert Einstein, 69621 Villeurbanne cedex, France
matthew.edwards@matelys.com

ABSTRACT

This work presents a prediction model for rolling noise in multi-story buildings, such as that generated by a rolling delivery trolley. Until now, mechanical excitation in multi-story buildings has been limited to impact sources such as the tapping machine. Rolling noise models have been limited to outdoor sources such as trains and automotive vehicles. The model presented here is able to predict the normalized sound pressure level in the reception room below generated by a trolley rolling in the emission room above, as well as the relative sound benefit of adding a covering to the floor upon which the trolley is rolling. The model can also represent the physical phenomena unique to indoor rolling noise, taking into account influencing factors such as the roughness of the wheel and the floor, the material and geometric properties of the wheel and the floor, the rolling velocity of the trolley, and the load on the trolley. The model may be used as a tool to investigate how different flooring systems (including multi-layer systems) respond to rolling excitation, for the purpose of developing multi-story building solutions which are better equipped to combat this kind of noise source.

1. INTRODUCTION

Structure-borne noise insulation is a field of building acoustics which has seen a large amount of research in recent decades. By far and away, the most common method of evaluating a building's performance in mitigating structure-borne noise is linked to impact noise. This is done primarily through the use of a tapping machine [1], though other methods such as the rubber ball [2] (see appendix F), walking noise [3], and even rainfall noise [2] are sometimes used. Recommendations for prediction of upward and lateral radiation from airborne and structure-borne excitation in heavy-weight buildings exists as well [4]. No standard currently exists for transmission to adjacent rooms for light-weight buildings. However, other sources exist beyond these, such as rolling noise.

Indoor rolling noise can take many forms: rolling office chairs, children's toys, and suitcases being a few examples of such structure-borne excitation sources. The most annoying, however, are possibly rolling trolleys or delivery carts, an example of which is shown in Figure 1.

Figure 1. A typical rolling delivery trolley.

Figure 2 shows the acoustic excitation due to a typical tapping machine and a typical rolling trolley on a classical concrete floor, in addition to the attenuation of a classical floating floor. The spectrum of impact noise is quite different than that of rolling noise, having the majority of its acoustic energy in the low frequency range. Furthermore, the attenuation of a classical floating floor is inverse to said rolling noise profile. As such, it does not provide sufficient insulation on its own without additional treatment.

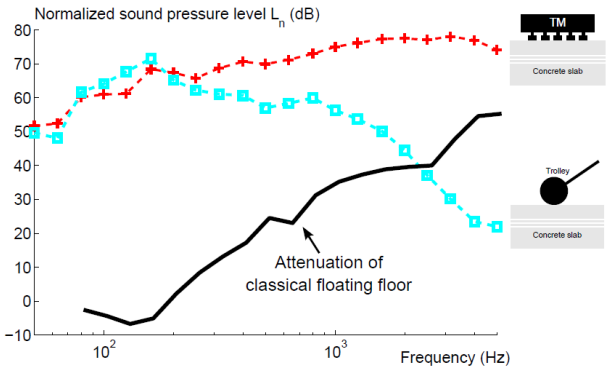

Figure 2. Comparison of the spectra of tapping noise and rolling noise of a classical concrete floor, as well as the attenuation of a classical floating floor (140 mm concrete slab + a decoupling layer + 40 mm screed) [5].

The difficulty in combating this type of structure-borne noise is that, because its sound signature is starkly dif-

ferent than that of impact noise, the solutions developed to help against impact noise can be sometimes ineffective against rolling noise. Additionally, impact noise modeling techniques cannot accurately predict the level of rolling noise generated in the same environment. For this reason, a unique method of modeling and predicting indoor rolling noise is needed.

Rolling noise has indeed been thoroughly investigated for decades, but uniquely in the context of vehicle tire/road and train wheel/rail contact. Models which aim at predicting these types of noise exist (see for example [6–8] for tire and [9–12] for train), but they cannot be easily adapted to work for indoor rolling noise due to differences in the underlying phenomena which cause such noise (mainly the propagation of the sound to the surrounding environment, which is quite different between roads, trains tracks and indoor buildings).

Previously, we developed a simple model for predicting rolling noise in an indoor environment [5, 13]. This model calculates the contact force between the wheel and the floor in the time domain, and uses it as the injected force into the floor to predict the resulting radiated sound power. Here we present an improved version of this model, which greatly expands in scope and application the capabilities of predicting indoor rolling noise. The improved model is capable of accounting for floors of various types and layered constructions, as well as discrete irregularities (beyond small-scale surface roughness) such as wheel flats and floor joints. In the sections that follow, the model is presented, along with a comparison with experimental test results.

2. MODEL DEVELOPMENT

Figure 3 shows the general outline of the rolling noise model. Operating in the time domain and in three spatial dimensions, the model uses the influencing properties of the wheel and floor to calculate the contact force between the two bodies for each discretized moment in time throughout the rolling event. These include the wheel and floor roughness profiles, the wheel and floor material properties (Young's modulus and Poisson's ratio), the speed of the trolley, the mass of the trolley (plus added load), and geometric profiles of the wheel and floor. Such profiles include not only the dimensions of the wheel, but also any discrete irregularities such as wheel flats or floor joints.

The contact force at each discretized moment in time is used as input into the dynamic model, where the resulting movement of the wheel and floor are calculated in response to the excitation injected force. This influences what the exact roughness profile will be for the following time step, as the wheel and floor continuously move in relation to one another, influencing how much (or how little) contact exists between them. Once the contact force has been calculated for each time step in the rolling event, the model is converted to the frequency domain, where the blocked force spectra is used in conjunction with the wheel and floor impedances to convert the blocked force to an injected force. From there the resulting radiated sound power may be calculated in the reception room through use of the transfer matrix method.

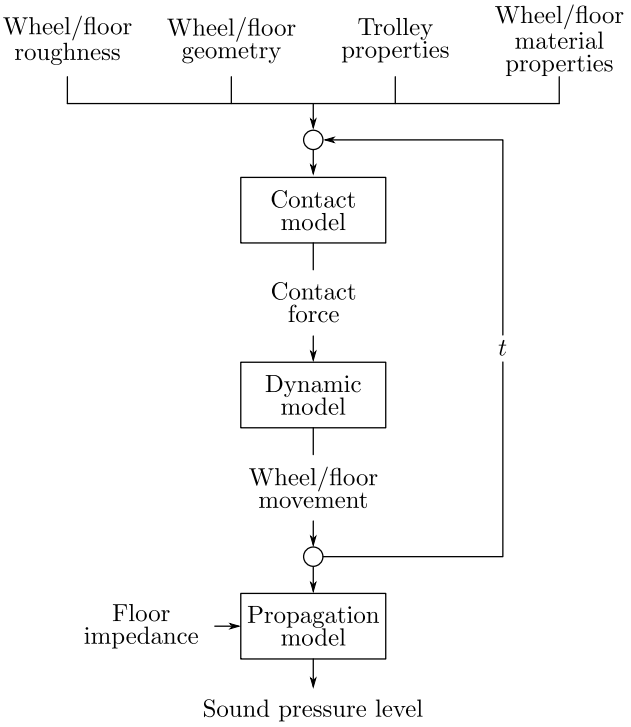

Figure 3. General outline of the rolling noise model.

2.1 Dynamic Model

The dynamic model, shown in Figure 4, is based on a wheel modeled as a spring-mass damper system resting on a rigid floor. The mass M is the mass of the trolley plus added load, divided by the total number of wheels on the trolley. The stiffness K is the equivalent elastic stiffness of the wheel, which is a function of the wheel's geometry and elastic properties. A presentation of how such a stiffness is calculated is given in [14]. A small amount of viscous damping C is added to be able to tune the model and avoid instabilities. The wheel is represented by its receptance $G_W(f)$ and Green's function $g_W(t)$, which are a measure of the wheel's vertical displacement in response to an impulse force input.

$$G_W(f) = \frac{1}{-(2\pi f)^2 M + i(2\pi f)C + K} \tag{1}$$

$$g_W(t) = \mathscr{F}^{-1}\left(G_W(f)\right) \tag{2}$$

where $\mathscr{F}^{-1}$ represents the inverse Fourier transform.

2.2 Contact Model

In order to estimate the contact force for each time step, a Winkler bedding is used. This has been used in other rolling noise models (for example [15,16]), and has proven to be a good estimation when compared to the more physically accurate Boussinesq method [17]. Figure 5 shows a diagram of the contact model, which is governed by the

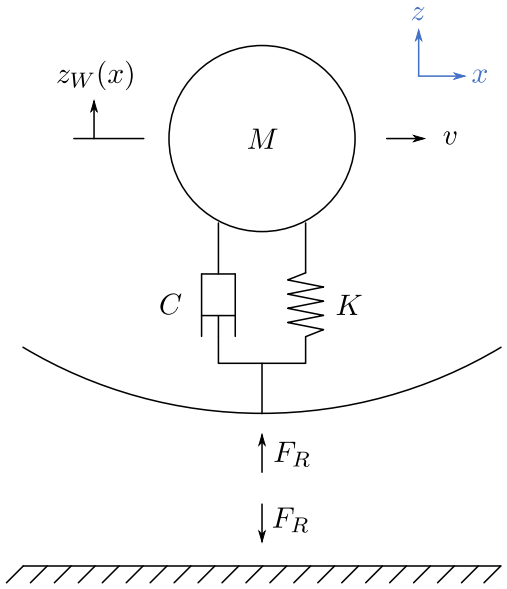

Figure 4. Dynamic model of the wheel/floor contact.

following equations

$$u'_R(x,x',y') = u_0 - z_W(x) - \varsigma(x,x',y') - \xi_W(x,x',y') + \xi_F(x,x') \quad (3)$$

$$\varsigma(x,x',y') = \varsigma_F(x,x',y') - \varsigma_W(x,x',y') \quad (4)$$

$$\sigma_R(x,x',y') = \begin{cases} \sigma_0\sqrt{\frac{u'_R(x,x',y')}{u_0}} & u'_R(x,x',y') > 0 \\ 0 & u'_R(x,x',y') \leq 0 \end{cases} \quad (5)$$

$$F_R(x) = \int\int \sigma_R(x,x',y')dx'dy' \quad (6)$$

$$z_W = g_W(1)(F_R(x) - Q) + g_W * (F_R - Q) \quad (7)$$

$$x = vt \quad (8)$$

A bed of independent, locally reacting springs is placed between the wheel and the floor, and their deflection used to estimate the stress profile σ_R in the area of contact for each time step t. The time step is converted to a position step by use of the trolley speed v.

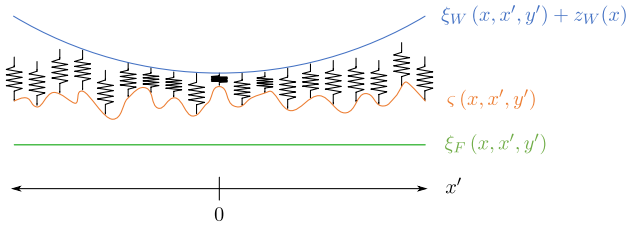

Figure 5. Contact model used for estimating the contact stresses between the wheel and the floor

The geometry of this interaction is determined by the total interpenetration profile u'_R between the floor and the wheel at a given wheel center position x, which is made up of the static Hertzian interpenetration in the absence of roughness (constant for all x), the wheel profile ξ_W, floor profile ξ_F, and relative roughness profile ς. The relative roughness profile is a difference of the individual wheel and floor roughness profiles at a given x.

Harris provides a thorough explanation of the static Hertzian deflection u_0 in [18] (see chapter 6). For a cylindrical wheel rolling on a flat floor, the deflection is

$$u_0 = \frac{4Q}{E'\pi w} \quad (9)$$

where Q is the effective mass M expressed as a load in Newtons, w is the wheel width (in the y direction), and E' is the apparent Young's modulus between the wheel and the floor, defined by

$$E' = \left(\frac{1-\nu_W^2}{E_W} + \frac{1-\nu_F^2}{E_F}\right)^{-1} \quad (10)$$

where E and ν are the Young's modulus and Poisson's ratio of the wheel and floor (denoted by the appropriate subscripts).

Typically, the wheel profile will be simply defined by it's radii of curvature,

$$\xi_W(x,x',y') = \frac{x'^2}{2r'_x} + \frac{y'^2}{2r'_y} \quad (11)$$

The floor profile will typically be zero for all x. However, in the presence of discrete irregularities such as wheel flat spots or floor joints, they may differ.

In order to ensure agreement with Hertzian contact mechanics, the wheel radii (both longitudinal r_x and transverse r_y) need to be reduced by unique factors which depend on the wheel's geometry, yielding reduced radii r'_x and r'_y. A full explanation is again given in chapter 6 in [18]. For a cylindrical wheel, the reduction is one half the original wheel radius. This modified radius must be used when defining the wheel profile ξ_W.

For a given moment in time, the wheel center is at a position x in the global coordinate system. The local coordinate system is positioned such that $x'(0) = x$, thus the origin of the local system follows the wheel center in the x dimension. For a given x, the roughness profile ς, wheel profile ξ_W and floor profile ξ_F are re-defined for the local coordinate system.

At a given position x, the contact stress profile σ_R may be calculated using the total interpenetration profile u'_R at said position. This is done in a manner similar to that which was used in [9], where the force in a given contact spring is set to change with the square root of its deflection in order to agree with Hertzian contact mechanics. In the discretized area between the wheel and the floor across which the calculation is performed, any points found to have negative stresses are assumed to be out of contact, and are thus set to zero. The stress profile may then be integrated across the entire contact area to obtain the full contact force due to roughness $F_R(x)$.

Once the contact force is known, the vertical wheel position z_W may be calculated using a convolution of the dynamic contact force and the wheel Green's function g_W

(represented in Equation (7) by the symbol $*$). This results in an interdependency of Equations (3) and (5) to (8). To alleviate this, the vertical wheel position at x is used to calculate the total interpenetration profile at $x + \Delta x$. For position $x = 0$, a vertical wheel position of $z_W(0) = 0$ is assumed.

Using this procedure, the wheel/floor interpenetration, contact force, and resulting wheel movement may be calculated for each position. At the end of the rolling event, the entire response history of the wheel and the floor is known.

2.3 Discrete Irregularities

Wheel flats are accounted for in the rolling noise model by modifying the wheel profile ξ_W at each discretized time step. For a wheel of radius r, an ideal wheel flat may modeled as a chord of the wheel circumference, as shown in Figure 6. The flat depth h_W, ideal flat length $l_{0,W}$, and ideal center angle Φ_0 are related by [19]

$$\frac{\Phi_0}{2} = \sin^{-1}\left(\frac{l_{0,W}}{2r}\right) = \cos^{-1}\left(1 - \frac{h_W}{r}\right) \tag{12}$$

The profile of such a wheel may be described by

$$R_{0,\phi}(\phi) = \begin{cases} r & |\phi| > \left|\frac{\Phi_0}{2}\right| \\ \frac{r\cos\frac{\Phi_0}{2}}{\cos\phi} & |\phi| < \left|\frac{\Phi_0}{2}\right| \end{cases} \tag{13}$$

where ϕ is evaluated over the interval $[-\pi, \pi]$.

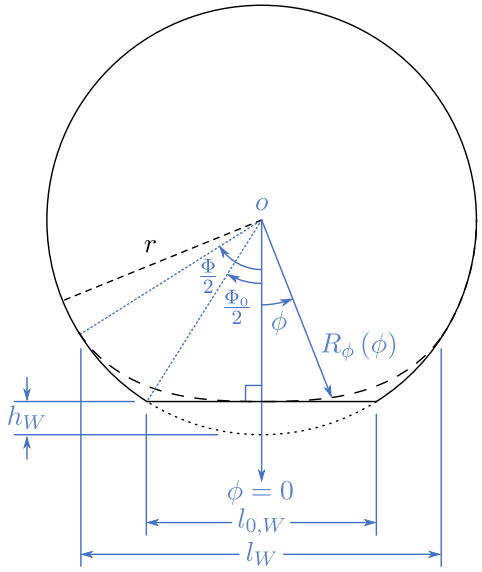

Figure 6. Geometry of an ideal and rounded wheel flat.

Alternatively, some rolling noise models have had success using a rounded wheel flat profile, which replaces the hard corner transition between flat and curved with one which has a more gentle profile [19–21]. This is intended to represent a wheel flat which has been in place for a period of time, and which has had its edges "worn down" from its ideal profile. Such a rounded profile may be represented by [19]

$$\frac{\Phi}{2} = \sin^{-1}\left(\frac{l_W}{2r}\right) = \cos^{-1}\left(1 - \frac{h_W}{r}\right) \tag{14}$$

$$R_\phi(\phi) = \begin{cases} r & |\phi| > \left|\frac{\Phi}{2}\right| \\ R - \frac{h_W}{2}\left[1 + \cos\left(\frac{2\pi\phi}{\Phi}\right)\right] & |\phi| < \left|\frac{\Phi}{2}\right| \end{cases} \tag{15}$$

One may recall that the wheel radius r_x is modified in the contact model in order to keep agreement with Hertzian contact mechanics and account for the non-linear deflection of the contact springs. Consequently, in order to map the flat spot to the wheel of reduced radius r'_x, the flat height is reduced here by the same amount.

$$h'_W = h_W \frac{r'_x}{r_x} \tag{16}$$

Similarly, the reduction of the wheel radius implicitly means that the wheel will make a greater number of revolutions across the floor for a given rolling event than what occurs in reality. This will result in an increase in the number of wheel flat impacts over a given rolling distance (in the case of a cylindrical wheel, the number of impacts will increase by a factor of two). This is corrected for by the following relation.

$$\Delta\phi = \frac{\Delta x}{r_x} \tag{17}$$

where Δx is the spatial resolution of the interpenetration profile in the global coordinate system, and $\Delta\phi$ is the angular spacing of the wheel profile at a given moment in time t in polar coordinates.

At each discretized time step in the model, the formulation of ξ_W used in Equation (3) is updated as the wheel flat moves through the vicinity of the contact area.

A similar approach is taken to account for the presence of floor joints in the rolling model. As shown in Figure 7, this is added directly into the rolling model by defining the floor profile in the global coordinate system (x, z) as the joint depth $-h_F$ within $\pm l_F/2$ of the joint center, and zero everywhere else. The joint centers are known based on the total rolling distance L and the length of an individual floor tile. Just as the wheel flat height was multiplied by r'_x/r_x in order to correctly map the flat profile to the reduced wheel radius, the same procedure is applied here, but this time to the floor joint length l_F.

$$l'_F = l_F \frac{r'_x}{r_x} \tag{18}$$

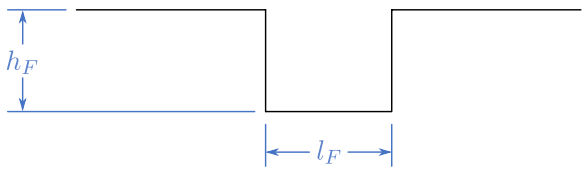

Figure 7. Geometry of a simple floor joint.

2.4 Propagation Model

The propagation model operates in the frequency domain to convert the previously calculated contact force and

wheel response to a radiated sound power. This is done using [22]

$$\Pi_{\text{rad}} = \frac{1}{8\pi^2}\int_0^{2\pi}\int_0^{\infty}\left(\left|\frac{F_{\text{flex}}(f)}{F_{\text{ref}}}\right|^2 \frac{Z_0\sigma_{\text{finite}}}{\left|Z_{\text{sTMM}}(f)+Z_{B,\infty}(f)\right|^2}k_r\mathrm{d}k_r\mathrm{d}\phi\right) \quad (19)$$

where F_{flex} is the injected force, F_{ref} is a reference force of 1 N, Z_0 is the acoustical impedance of air, Z_{sTMM} is the impedance of the multilayered floor, $Z_{B,\infty}$ is the radiation impedance, and σ_{finite} is the "finite size" radiation efficiency. The transfer matrix method (TMM) is used to calculate the impedance of the multilayered floor Z_{sTMM} for each wavenumber couple (k_x, k_y) or (k_r, ϕ). In essence, the radiated power of an infinite plate is calculated, then spatially windowed to achieve the effective radiation of a plate with size equal to the actual floor.

The injected flexural force F_{flex} depends on the blocked force, which is taken to be the contact force $F_R(f)$. This takes into account the impedance of both the wheel and floor, using

$$|F_{\text{flex}}(f)|^2 = \left|\frac{Z_{\text{sTMM}}(f)}{Z_{\text{sTMM}}(f)+Z_{\text{exc}}(f)}\right|^2 |F_R(f)|^2 \quad (20)$$

Where Z_{exc} is the wheel impedance, estimated as the blocked force divided by the time derivative of the vertical wheel position.

As with the wheel impedance, the floor impedance may theoretically be calculated by dividing the injected force by the floor velocity. However, as the injected force in calculated from the contact force found in the contact model, it may appear that it cannot be known ahead of time. To alleviate this problem, the floor impedance is pre-calculated using an injected point force of 1 N. This essentially yields a unit floor impedance, which when used in Equation (20) in conjugation with the blocked force, will yield the correct injected flexural force.

3. ROUGHNESS MEASUREMENT

In order to provide an accurate estimation of the relative roughness between the wheel and the floor as input to the rolling noise model, roughness samples from two cylindrical wheels and three floors were measured. This was done using a Nikon LC15DX 3D scanner with an average spatial resolution of 22 µm.

The floors measured were polished concrete, a smooth PVC floor covering, and a rough PVC floor covering. The two PVC floors were identical in construction, the only difference being their surface roughness. A 3.5 cm wide section was measured along the full length of each floor sample: 20 cm for the concrete and 60 cm for the PVC.

The two wheels were identical in material composition and overall geometry ($r = 5$ cm, $w = 3.5$ cm), with the difference being that one contained a series six of non-periodic flat spots around its circumference (each flat spot having a depth of 0.5 mm). The entire rolling surface was captured, giving a width equal to the wheel width, and length equal to the wheel's circumference.

4. EXPERIMENTAL RESULTS

The model was compared to experimental results gathered from a rolling noise test performed at Level Acoustics and Vibration in Eindhoven, the Netherlands. The sound generated by a rolling test trolley was captured in a two-story transmission room: with the trolley being rolled in the top (emission) room, and the sound measured in the bottom (reception) rooms. The measurement procedure outlined in ISO 10140-3 [1] for laboratory testing of a tapping machine was used. The two rooms were separated by a 10 cm thick concrete floor, which was decoupled from the surrounding floor to eliminate sound transmitted to the reception room via flanking transfer paths.

The test trolley used was a simple two-wheel design, as it allows the rolling noise itself to be accurately represented while eliminating all other sources of noise which are beyond the scope of this model (e.g. rattling noise). The three floor types and two wheel types which had their roughness profiles measured were tested, for a total of six wheel/floor combinations.

4.1 Normalized sound pressure level

The model and experimental results were first compared using their normalized sound pressure level in the reception room L_n, calculated from ISO 10140-3 [1]. This takes into account the absorption of the reception room in calculating the sound pressure level of the rolling trolley.

Figure 8 shows the model versus experimental results of the normalized sound pressure level in the reception room due to the two-wheeled rolling test trolley for the smooth wheel, ideal flat wheel, and rounded flat wheel on three floors: bare concrete, concrete + rough PVC covering, and concrete + smooth PVC covering. For each of these tests, the mass of the trolley + added load was 17 kg. The trolley was rolled at an average rate of 0.9 m/s in a linear trajectory. The trolley was rolled back and forth repeatedly for a period of 30 seconds, and the sound averaged over the entire time span for each run. A total of 5 runs were performed and averaged together for each unique configuration in order to elimination variations in repeatability between runs. The concrete floor generally yields higher levels than the rough and smooth PVC floors, which are similar to one another in shape and magnitude. Considering the only difference between these two floors is their surface roughness, we may conclude that in the case of soft materials, surface roughness plays less of a role in determining the overall sound level than other factors such as the elasticity of the floor. Model results agree well above 300 Hz for the ideal flat wheel. The smooth wheel and rounded flat wheel tend to under-predict across the whole frequency range, however their general shapes are still congruent with those of their respective experimental curves. The background noise level for the measurement was set

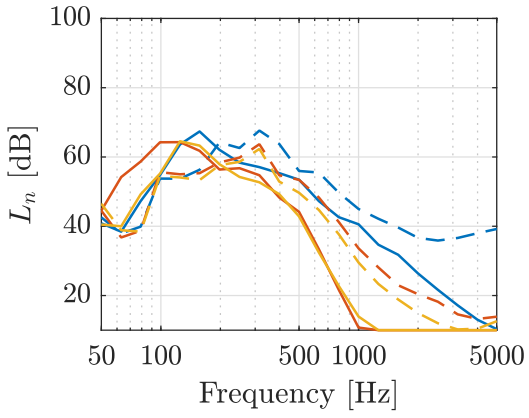

(a) Smooth wheel

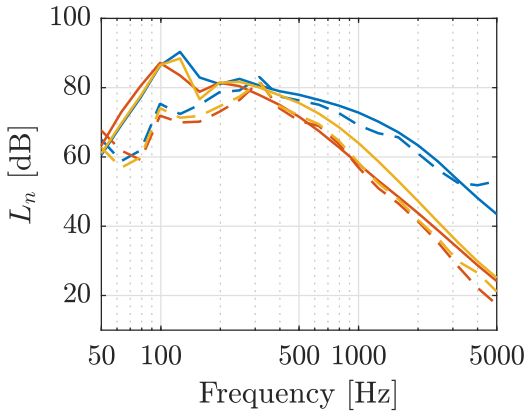

(b) Ideal flat wheel

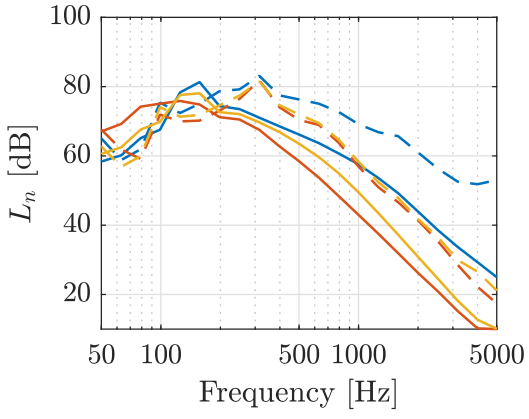

(c) Rounded flat wheel

Figure 8. Normalized sound pressure level in the reception room for varying floor covering: model versus experiment. For all curves, the trolley speed was 0.9 m/s and the added load was 10 kg. — model concrete floor, - - - experiment concrete floor, — model, rough PVC floor, - - - experiment, rough PVC floor, — model smooth PVC floor, - - - experiment, smooth PVC floor.

to 10 dB, so any values below this were corrected to this level. This can be seen particularly in the results for the smooth wheel above 1 000 Hz.

4.2 Relative normalized sound pressure level

An alternative way of visualizing the data is to calculate the reduction in normalized sound pressure level ΔL_n [1]. This is found by subtracting the L_n with a floor covering in place from the L_n of bare concrete. This is done not only because the benefit of a floor covering is often the primary quantity of interest, but also because doing do helps remove variations in experimental data, as well as modeling uncertainties, which may be present in the absolute level results.

Figure 9 shows the benefit of adding a floor covering, as computed with both model and experimental data. There is quite a bit less difference between the three wheel types in the ΔL_n plots than in the L_n plots, indicating that the floors provide more or less a similar benefit regardless of wheel type. Additionally, while the model is not perfectly accurate at estimating the absolute sound level L_n, it is much more accurate at estimating the reduction in sound level ΔL_n. A greater deviation occurs in the high frequency range for the smooth wheel, where the model has a tendency to over-predict above 500 Hz. This is due to the weak excitation of the smooth wheels. The curves shown here were not corrected to the background noise level of 10 dB, so the behavior of the curves in the high frequency range are true to reality.

5. DISCUSSION

The primary objective of this work was to develop a rolling noise model that can capture the physical phenomena present in indoor rolling contact, as well as predict the sound level benefit of adding a floor covering to a given floor. The model which was developed has been specifically adapted for the characteristics of rolling in multi-story buildings, such as highly elastic wheels, multi-layer floors, and sound propagation via vertical structure-borne transfer paths. This is a domain which has hereto been left unexplored. As such, it serves as a ground-breaking look into the problem of indoor rolling noise. This work may be a platform to spur further exploration into the field of indoor rolling noise.

An important observation to make when comparing the two plots in Figure 8 is that, while the addition of a PVC floor covering aids in reducing the overall noise level for a given wheel, the flat wheel on PVC is still louder than the smooth wheel on bare concrete. This validates the necessity for a model which is capable of accounting for discrete irregularities, as their presence can quickly eliminate any benefit that a quieter material (whether for the floor or wheel) would provide. The smooth wheel does not always provide a sufficient signal to noise ratio for precise measurements, particularly in the presence of a soft floor covering.

Using a model such as the one presented here, the acoustic performance of various floor systems may be estimated in order to identify which ones yield the greatest benefit for rolling noise. This is a technique which already exists for other sources of indoor structure-borne

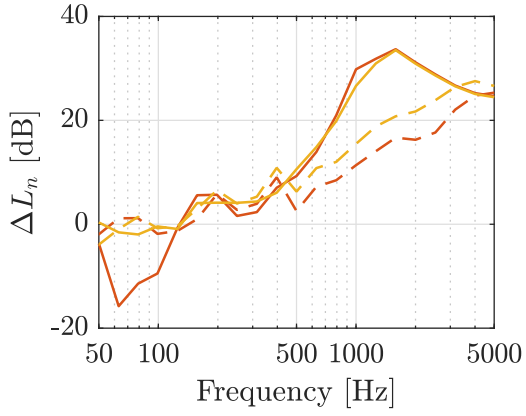

(a) Smooth wheel

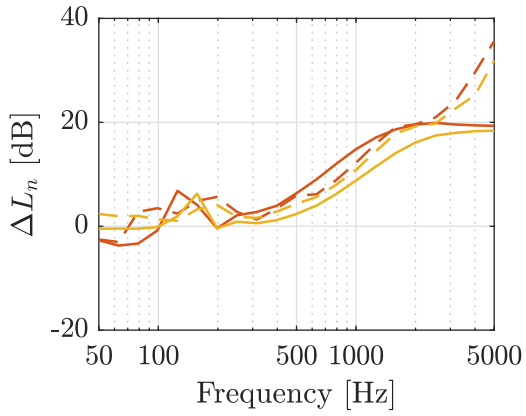

(b) Ideal flat wheel

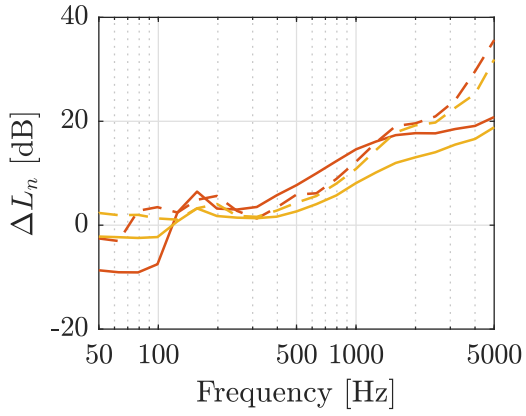

(c) Rounded flat wheel

Figure 9. Benefit from applying the rough and smooth PVC floor coverings: model versus experiment. For all curves, the trolley speed was 0.9 m/s and the added load was 10 kg. — model concrete floor, - - - experiment concrete floor, — model, rough PVC floor, - - - experiment, rough PVC floor, — model smooth PVC floor, - - - experiment, smooth PVC floor.

noise, such as the tapping machine. However, because impact noise is starkly different than rolling noise, floor systems which have been developed for reducing impact noise will not necessarily exhibit high performance with rolling noise as well. This model may serve as a complement to the existing indoor structure-borne noise modeling solutions: aiding in the development of building materials which have better acoustic performance for a wider range of sound sources.

As is the case with any numerical model, the results are only as good as the inputs. In addition to the roughness profiles, experimental data regarding the elastic properties of the floor (in particular, the dynamic loss factor) are necessary for this model. It is known that the damping of the floor has a large effect on the transmitted structure-borne noise when being excited by a mechanical source [23]. While extensive measures were taken to obtain highly accurate roughness profiles, improved measurement of the wheel and floor material properties may provide greater accuracy in the overall model results.

The test trolley used was developed to produce a rolling sound which was as regular as possible: free of extraneous signatures such as rattling or other trolley vibrations. Just as there exists a standard tapping machine for normalizing the measurement process of impact noise across various test locations, the possibility of a standard rolling device also exists. The development of such a device could aid in the furthering the field of indoor rolling noise research, as it would allow a congruent means of comparing rolling noise measurements gathered in different scenarios. For further discussion on this topic, see [24].

6. CONCLUSION

This work presents an improved time-domain model for predicting rolling noise in buildings. The model is able to predict with relative accuracy the radiated sound power of a wheeled trolley rolling across a floor while accounting for the roughness of the floor & wheel, the elastic parameters of the floor & wheel, the speed of the trolley, and the load of the trolley. The model is also able to account for discrete irregularities, such as wheel flat spots and floor joints. A model such as this one may be used as a supplement to the existing models for floor impact noise, in order to test different wheel/floor material combinations to see which ones result in the greatest reduction in noise. It may also be used to identify trends in order to guide the development of new vibro-acoustic materials which are effective at both reducing both impact noise and rolling noise.

7. ACKNOWLEDGMENTS

This work was done as part of Acoutect: an innovative training network composed of 5 academic and 7 non-academic participants. This consortium comprises various disciplines and sectors within building acoustics and beyond, promoting intersectoral, interdisciplinary and innovative training and mobility of the researchers within the project. This project has received funding from the European Union's Horizon 2020 research and innovation program under grant agreement No 721536. This work was also performed within the framework of the Labex CeLyA of Université de Lyon, operated by the French National Research Agency (ANR-10-LABX-0060/ANR-11-IDEX-0007).

8. REFERENCES

[1] "ISO 10140-3:2010 - Acoustics – Laboratory Measurement of Sound Insulation of Building Elements – Part 3: Measurement of Impact Sound Insulation," 2010.

[2] "ISO 10140-5:2010 - Acoustics – Laboratory Measurement of Sound Insulation of Building Elements – Part 5: Requirements for test facilities and equipment," 2010.

[3] "BS EN 16205:2013+A1:2018 - Laboratory measurement of walking noise on floors," 2018.

[4] B. Asmussen, "Definition of appropriate procedures to predict exposure in buildings and estimate annoyance Deliverable D1.6," 2012.

[5] M. Edwards, F. Chevillotte, L. Jaouen, F.-X. Bécot, and N. Totaro, "Rolling Noise Modeling in Buildings," in *47th International Congress and Exposition on Noise Control Engineering (Internoise 2018): Impact of Noise Control Engineering*, (Chicago, IL USA), Aug. 2018.

[6] F. Wullens and W. Kropp, "A Three-Dimensional Contact Model for Tyre/Road Interaction in Rolling Conditions," *Acta Acust united Acust*, vol. 90, pp. 702–711, 2004.

[7] P. B. U. Andersson and W. Kropp, "Time Domain Contact Model for Tyre/Road Interaction Including Nonlinear Contact Stiffness due to Small-Scale Roughness," *J Sound Vib*, vol. 318, pp. 296–312, Nov. 2008.

[8] R. J. Pinnington, "Tyre–Road Contact Using a Particle–Envelope Surface Model," *J Sound Vib*, vol. 332, pp. 7055–7075, Dec. 2013.

[9] P. Remington and J. Webb, "Estimation of Wheel/Rail Interaction Forces in the Contact Area due to Roughness," *J Sound Vib*, vol. 193, pp. 83–102, May 1996.

[10] D. J. Thompson, B. Hemsworth, and N. Vincent, "Experimental Validation of the TWINS Prediction Program for Rolling Noise, Part 1: Description of the Model and Method," *J Sound Vib*, vol. 193, pp. 123–135, May 1996.

[11] D. J. Thompson, P. Fodiman, and H. Mahé, "Experimental Validation of the TWINS Prediction Program for Rolling Noise, Part 2: Results," *J Sound Vib*, vol. 193, pp. 137–147, May 1996.

[12] O. E. Lundberg, S. Finnveden, S. Björklund, M. Pärssinen, and I. Lopez Arteaga, "A Nonlinear State-Dependent Model for Vibrations Excited by Roughness in Rolling Contacts," *J Sound Vib*, vol. 345, pp. 197–213, June 2015.

[13] F. Chevillotte, F.-X. Bécot, and L. Jaouen, "Rolling noise model for building acoustics purposes," in *Euronoise 2015*, (Maastricht, the Netherlands), 2015.

[14] M. Edwards, F. Chevillotte, F.-X. Bécot, L. Jaouen, and N. Totaro, "Polynomial relations for cylindrical wheel stiffness characterization for use in a rolling noise prediction model," *Acta Acust.*, vol. 4, no. 2, p. 4, 2020.

[15] D. J. Thompson, "On the Relationship Between Wheel and Rail Surface Roughness and Rolling Noise," *J Sound Vib*, vol. 193, pp. 149–160, May 1996.

[16] A. Pieringer, W. Kropp, and J. Nielsen, "A time domain model for the wheel/rail interaction aiming to include non-linear contact stiffness and tangential friction," in *Proceedings of the 9th International Workshop on Railway Noise (IWRN9)*, (Munich, Germany), 2007.

[17] J. Boussinesq, "Application des Potentiels à l'Étude de l'Équilibre et du Mouvement des Solides Élastiques, Principalement au Calcul des Déformations et des Pressions que Produisent, dans ces Solides, des Efforts Quelconques Exercés sur une Petite Partie de leur Surface ou de leur Intérieur : Mémoire Suivi de Notes Étendues sur Divers Points de Physique Mathématique et d'Analyse (Application of the Potentials to the Study of the Equilibrium and Movement of Elastic Solids, Mainly to the Calculation of the Deformations and Pressures that Produce, in these Solids, Some Efforts Exercised on a Small Part of their Surface or Interior: Memory Followed by Extended Notes on Various Points of Mathematical Physics and Analysis.)," *Lilliad - Université de Lille - Sciences et technologies*, 1885.

[18] T. A. Harris and M. N. Kotzalas, *Rolling Bearing Analysis*. Boca Raton, FL: CRC/Taylor & Francis, 5th ed ed., 2007.

[19] A. Pieringer and W. Kropp, "A fast time-domain model for wheel/rail interaction demonstrated for the case of impact forces caused by wheel flats," in *7th European Conference on Noise Control 2008 (Euronoise 2008)*, (Paris, France), pp. 2643–2648, 2008.

[20] L. Baeza, A. Roda, J. Carballeira, and E. Giner, "Railway Train-Track Dynamics for Wheelflats with Improved Contact Models," *Nonlinear Dyn*, vol. 45, pp. 385–397, Aug. 2006.

[21] T. X. Wu and D. J. Thompson, "A Hybrid Model for the Noise Generation due to Railway Wheel Flats," *J Sound Vib*, vol. 251, pp. 115–139, Mar. 2002.

[22] D. Rhazi and N. Atalla, "Transfer Matrix Modeling of the Vibroacoustic Response of Multi-Materials Structures Under Mechanical Excitation," *J Sound Vib*, vol. 329, pp. 2532–2546, June 2010.

[23] F. Chevillotte, F.-X. Bécot, and L. Jaouen, "Analysis of Excitations from the Wavenumber Point of View," in *NOVEM 2015*, (Dubrovnik, Croatia), Apr. 2015.

[24] M. Edwards, R. G. Diaz, N. Dallaji, and L. Jaouen, "Recommendation for a Standard Rolling Noise Machine," *arXiv:2008.12053 [physics]*, Aug. 2020.